ANATOMIA HISTOLOGIA EMBRYOLOGIA
JOURNAL OF VETERINARY MEDICINE
Anatomia, Histologia, Embryologia

ORIGINAL ARTICLE

On the Cornea of Healthy Merino Sheep: A Detailed Ex Vivo Confocal, Histological and Ultrastructural Study

T. A. Cafaro[1†], M. F. Suarez[2†], C. Maldonado[3], J. O. Croxatto[4], C. Insfrán[2], J. A. Urrets-Zavalía[5†] and H. M. Serra[2*†]

Addresses of authors: [1] Faculty of Chemical Science, National University of Córdoba, Medina Allende, Córdoba, Argentina;
[2] Department of Clinical Biochemistry, CIBICI, Faculty of Chemical Science, National University of Córdoba, Medina Allende, Córdoba, Argentina;
[3] Centre of Electron Microscopy, Faculty of Medical Sciences, National University of Córdoba, Haya de la Torre, Córdoba, Argentina;
[4] Department of Ophthalmic Pathology, Fundación Oftalmológica Argentina Jorge Malbrán, Viamonte 1181, Buenos Aires, Argentina;
[5] Department of Ophthalmology, University Clinic Reina Fabiola, Catholic University of Córdoba, Oncativo 1248, Córdoba, Argentina

***Correspondence:**
Tel.: 54 351 4344973;
fax: 54 351 4333048;
e-mail: hserra@fcq.unc.edu.ar

With 7 figures and 1 table

Received April 2014; accepted for publication June 2014

doi: 10.1111/ahe.12131

[†]These authors equally contributed to this work.

Summary

Our study performed qualitative and quantitative studies on the corneal ultrastructure of healthy female Merino sheep of ages 4 months and 6 years old from the Argentinean Pampa. The corneas were evaluated using *ex vivo* laser-scanning confocal microscopy, light microscopy and transmission electron microscopy. Those studies allowed us to obtain detailed images of the corneal layers as well as quantitative data of the cellular and sub-basal nerve densities in the cornea from sheep of different ages. The density of the corneal cells was significantly different in the anterior versus the posterior epithelium and stroma. Moreover, the density of the epithelial, stromal cells and endothelial cells, as well as the sub-basal nerve density were significantly lower in adult than in young animals. Our work provided a wide-ranging description of the corneal ultrastructure of healthy female Merino sheep, which adds to the current knowledge about the ophthalmological aspects of this species and undoubtedly benefits veterinarians.

Introduction

In Argentina, sheep are bred predominantly for the production of wool, with meat only considered to be a by-product as their carcass size is generally smaller than that of animals usually bred for meat. There are three geographically and climatologically different Argentinean sheep breeding regions, namely Puna, Patagonia and the Pampa (together with Mesopotamia, Uruguay and South Brazil) (Cardellino, 1989).

Very few studies have described the ophthalmological features of sheep. To the best of our knowledge, the first description of the anterior segment of sheep's eye was published in 1960 by Prince. Much later, Scott and Bosworth published in 1990 a comparative biochemical and ultrastructural examination of the proteoglycan–collagen interactions in the corneal stroma between sheep and other species (Scott and Bosworth, 1990). Galan et al. (2006) then reported similarities and differences in the ocular fundus between sheep and goat eyes, and the use of an endoscopic technique allowed Guyomard et al. (2008) to obtain a circular view of the anterior (iridocorneal angle) eye segment of sheep and other animal species. More recently, Reichard et al. (2010) using *in vivo* corneal confocal microscopy (CCFM), studied the corneal anatomy of a Pomeranian Coarsewool sheep and that of other laboratory animals.

Our present investigation was conducted to describe the ultrastructural characteristics of the corneas of young and adult healthy female Merino sheep grazing in the Pampa region of Argentina. Our data provided additional information and details of this species corneal structures, which adds to the present knowledge about the ophthalmological aspects of sheep and will undoubtedly benefit veterinarian.

Methods

Healthy female Merino sheep of different ages, bred in a central region of Argentina and free of macroscopically observable alterations to the cornea, were included in this study. All procedures were in accordance with The Faculty of Chemical Science Animal Research Act and the Association for Research in Vision and Ophthalmology (ARVO), Statement for the Use of Animals in Ophthalmic and Vision Research.

Animals aged 4 months old ($n = 3$) and 6 years old ($n = 3$), which had a normal corneal appearance based on slit-lamp bio-microscopy studies performed both before and after fluorescein staining, were slaughtered and their eyes removed. The left eye from each animal was preserved in a wet chamber at 4°C for *ex vivo* laser-scanning confocal microscopy (EVCM) studies, and the right eye was processed for histological evaluation.

EVCM was performed 5 h after the ewes' eyes were removed with a Rostock Cornea Module/Heidelberg Retina Tomograph II (Heidelberg Engineering GmbH, Heidelberg, Germany). The examination was performed with the whole globe held in front of the microscope by a clamp holder, with images through all the layers of the central cornea being obtained, digitally stored and then analysed using image processing and analysis software programs as previously described (Al-Aqaba et al., 2010). The corneal epithelial, stromal, and endothelial cell densities (cell/mm^2) and sub-basal nerve density (total length of all nerve fibres and branches within a frame in μm/mm^2) were determined (Patel et al., 2009; Al-Aqaba et al., 2010).

The corneas from the right eyes were cut into two pieces and processed for light microscopy (LM) and transmission electron microscopy (TEM). One piece was fixed in phosphate buffer saline (PBS) – formaldehyde (10% v/v) (24 h), dehydrated and embedded in low-temperature paraffin wax. Serial sections (6 μm) were cut, mounted on 0.1% poly-L-lysine-coated slides, dried overnight at 37°C, stained with haematoxylin and eosin (HE). The morphology of the cornea in the central and peripheral regions was examined using light microscopy (Nikon ACT-2U; A.G. Heinze, Tokyo, Japan). Images were taken with a digital camera (Nikon Sight DS-U; A.G. Heinze) and thickness measurements of the whole cornea and epithelium were made using a calibrated object micrometre.

The other piece was fixed by immersion in Karnovsky's mixture containing 1.5% glutaraldehyde (v/v) and 4% paraformaldehyde (w/v) in 0.1 M cacodylate buffer. Samples from the cornea were post-fixed in 1% osmium tetroxide, dehydrated and embedded in Araldite. For high-resolution light microscopic examination (HRLM), 1 μm-thick sections were cut with a glass knife on a Porter-Blum MT2 ultra-microtome, stained with 1% alkaline toluidine blue and observed with an optical microscope (Nikon ACT-2U; A.G. Heinze) using magnifications of ×40 and ×100. For ultrastructural studies, thin sections were cut with diamond knives in a JEOL JUM-7 ultra-microtome and mounted on nickel grids. After being counterstained with uranyl acetate and lead citrate, sections were examined using a Zeiss LEO 906E electron microscope (Carl Zeiss, Oberkochen, Germany).

Statistical analysis was carried out using the nonparametric Mann–Whitney *U*-test, with data presented as means ± SD and $P < 0.05$ being taken as the threshold of statistical significance.

Results

All the images shown in this manuscript correspond to adult sheep corneas with the exception of images observed in Fig. 3 where EVCM pictures corresponding to young and adult animals can be seen side by side.

Ex vivo studies

A complete description of the corneal layers was accomplished using EVCM. Quantitative data from the sheep corneas for the parameters examined are summarized in Table 1, where it can be observed that the basal cell

Table 1. EVCM quantitative results of sheep corneal cells and sub-basal nerves

Corneal components	4 month old sheep $n = 3$ Cellular density (cell/mm^2) Mean ± SD	6-year-old sheep $n = 3$ Cellular density (cell/mm^2) Mean ± SD
Epithelium		
Surface cells	457 ± 76	490 ± 69
Superficial wing cells	2016 ± 232.5[c]	1231 ± 89
Intermediate wing cells	3035 ± 575.2	3830 ± 421.3
Basal cells	5491 ± 406.2[a,c]	4431 ± 492.5[a]
Stroma		
Anterior stromal cells	466 ± 46.1[b,c]	300 ± 45.6[b]
Posterior stromal cells	236 ± 52.4	180 ± 39.9
Endothelium	3713 ± 502.4[c]	2032 ± 69.8
	Sub-basal nerves density (μm/mm^2) Mean ± SD	Sub-basal nerves density (μm/mm^2) Mean ± SD
Sub-basal nerves	8672 ± 798[c]	4249 ± 308

[a]$P < 0.05$ (basal versus intermediate cells, and basal versus superficial cells).

[b]$P < 0.05$ (anterior versus posterior stromal cells).

[c]$P < 0.05$ (4 months old versus 6 years old).

density was significantly higher than that of the intermediate and superficial cells in the epithelium ($P < 0.05$), while the density of the stromal cells was significantly lower in the posterior than in the anterior stroma ($P < 0.05$). The cellular density of some types of epithelial cells (superficial wing cells, basal cells) was significantly higher in 4-month-old sheep compared with 6-year-old ones ($P < 0.05$).

A representative oblique image of the epithelium and anterior stroma of the sheep cornea is shown in Fig. 1a. As expected from normal histology, the epithelium was composed of three distinct layers: superficial, intermediate (wing cell layer) and basal layers. The superficial epithelial cells displayed a haphazard arrangement of large polygonal and sometimes hexagonal cells, with both hyper-reflective or hyporeflective cytoplasms and small round hyper-reflective nuclei surrounded by a clear hyporeflective halo. The hyper-reflective cytoplasm, presumably related to the loss of organelles and a compact arrangement of keratin proteins, was more conspicuous in desquamated cells (Fig. 1b). Intermediate polygonal cells had a dark cytoplasm, with hyper-reflective cell boundaries, due to the presence of numerous desmosome complexes. The intermediate cell layer displayed progressively smaller cells from the most superficial to the deeper layers. There also appeared to be more than one layer of regular small basal cells, with the upper layer containing small hyper-reflective dots (Fig. 1c) and other layer of cells having a dark cytoplasm and hyper-reflective cell boundaries (Fig. 1d).

Although the Bowman layer was not observed, a sub-basal nerve plexus and stromal nerves were easily detectable (arrows in Fig. 2a,b,c). As shown in Table 1, the sub-basal nerve density was significantly lower in 6-year-old animals than in 4-month-old sheep ($P < 0.05$).

The stroma's extracellular matrix was irregularly reflective with numerous reflective stellate-shaped stromal cells with visible but poorly defined nuclei observed in the anterior stroma (Fig. 2b). The deeper stromal cells displayed an elongated configuration, but again with barely visible nuclei (Fig. 2c). Significant differences in anterior stromal cell densities were found among animals of dissimilar ages ($P < 0.05$, Table 1).

A dark transition zone (Descemet's membrane) between the posterior stroma and the endothelial cells was also observed. The endothelium revealed hyper-reflective cells with dark boundaries and central hyporeflective nuclei organized in a honeycomb pattern with minimal

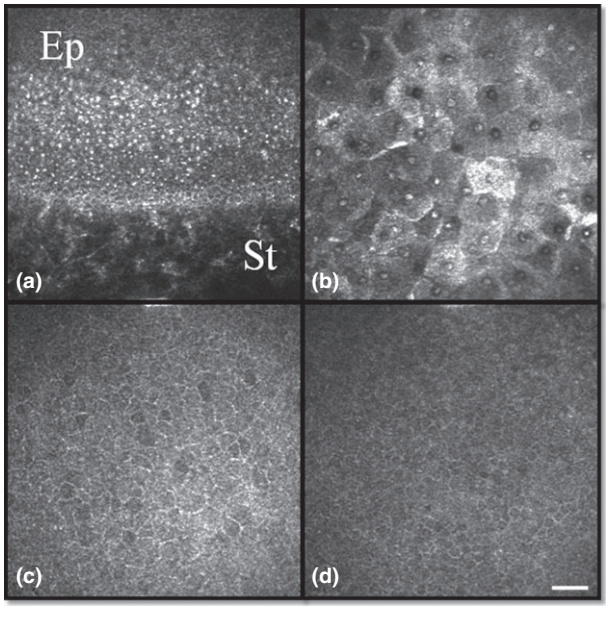

Fig. 1. *Ex vivo* laser-scanning confocal microscopy images: (a) oblique section of sheep cornea showing the epithelium and anterior stroma; (b) superficial epithelium; (c) The upper layer of basal cells containing small hyper-reflective dots; (d) basal epithelium. Ep, epithelium; St, stroma. Original magnification: 400 × 400 μm, Bar 50 μm.

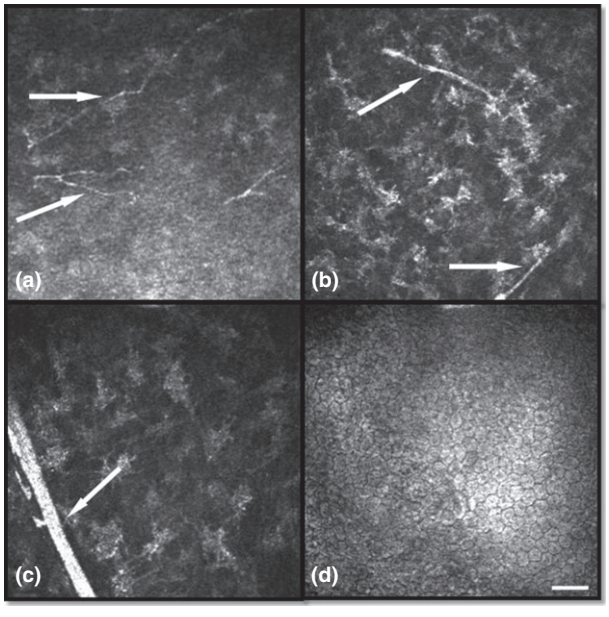

Fig. 2. *Ex vivo* laser-scanning confocal microscopy images. (a) superficial nerve plexus between basal cells and anterior stroma in oblique image; corneal nerves were seen as hyper-reflective thin linear structures (arrows); (b) in the anterior stroma, extracellular matrix was irregularly reflective; numerous reflective star-shaped stromal cells with no clearly visible nuclei and corneal nerves (arrows); (c) posterior stroma with reflective structures and thicker nerves; (d) the endothelium showed hyper-reflective cells with dark boundaries and central hyporeflective nuclei. The endothelial cells displayed minimal variation in shape or size and were organized in a honeycomb pattern. Original magnification: 400 × 400 μm, Bars 50 μm.

variations in shape or size (Fig. 2d), with there being a significant decrease in the number of endothelial cells with increasing age of the sheep ($P < 0.05$, Table 1).

Representative images of the quantitative differences found between young and adult sheep can be seen side by side in Fig. 3.

In vitro studies

The evaluation of the cornea layers using LM and TEM was similar in both groups of animals. Total cornea and epithelium thicknesses in young and adult animals were 778.2 ± 12.37 μm versus 782.2 ± 10.47; and 80.22 ± 4.6 versus 77.66 ± 3.4, respectively. The stratified and non-keratinized epithelium was composed of five superficial cell layers, 5–6 layers of intermediate (wing) cells and 1–2 layers of basal cells (Fig. 4a,b). Superficial cells were polygonal, with an eosinophilic cytoplasm, flattened nucleus and with many cells undergoing desquamation and with the intermediate layer being formed by cuboidal cells with an ovoid nucleus. Basal cells were cubical with most of them being cylindrical, tightly grouped and bigger than the rest of the epithelial cells. The anterior apex was convex, with the nucleus located centrally in the cell, and on some occasions, a few mitosis observed. Below these cells, a basement membrane, a relatively thin Bowman's layer, a thick corneal stroma, a clear Descemet membrane and an endothelial cell layer were observed (Fig. 4a,b,c).

The corneal limbus was characterized by the presence of pigmented cells on the basal layer of the epithelium and anterior stroma (Fig. 5). The melanin-containing cells were observed in epithelial cells and in keratocytes, and they were irregularly distributed throughout the limbal circumference. The blood vessels appeared in the limbus but did not extend into the cornea (Fig. 4).

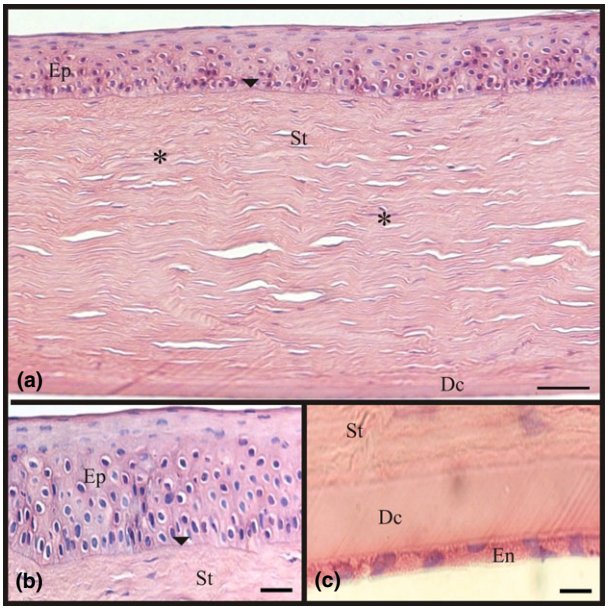

Fig. 4. Light microscopy images stained with haematoxylin–eosin (HE): (a) full-thickness section of central cornea stained with HE; different structures were recognized: the epithelium lying on the basement membrane (arrowhead), the stroma with keratocyte (*), the Descemet's membrane and the endothelium; (b) stratified epithelium on a basement membrane (arrowhead); (c) Descemet's membrane and endothelium. Ep, epithelium; St, Stroma; En, endothelium; Dc, Descemet's Membrane. Original magnifications (a): 40× Bars 100 μm; (b, c): 100× Bars 20 μm.

High-resolution LM and TEM allowed clear images of cornea epithelium layers to be observed with different activity grades and shapes (Fig. 6). The basal layer

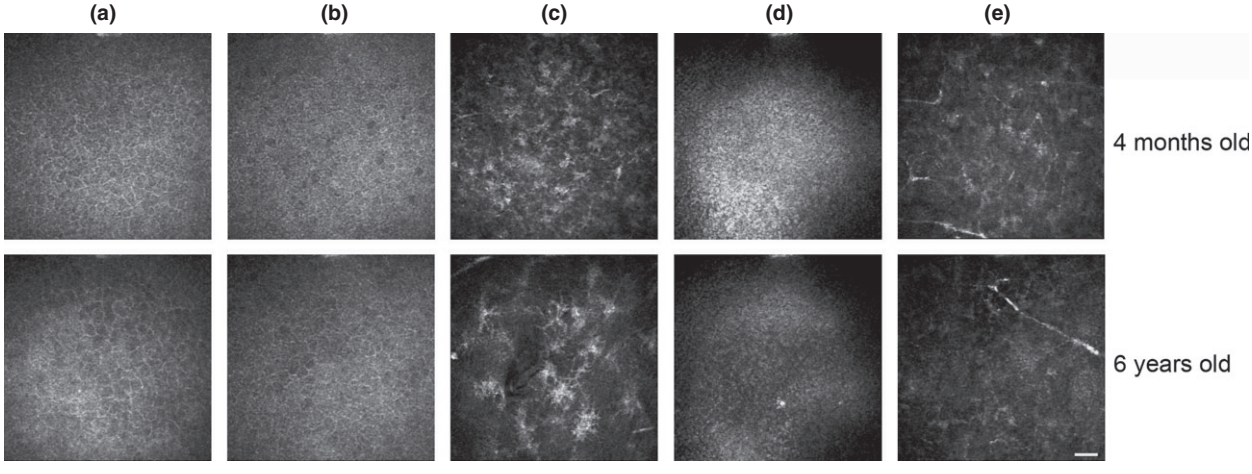

Fig. 3. *Ex vivo* laser-scanning confocal microscopy images of young and adult sheep. (a) superficial wings cells; (b) basal cells; (c) anterior stromal cells; (d) endothelial cells; (e) sub-basal nerves. Original magnification: 400 × 400 μm, Bar 50 μm.

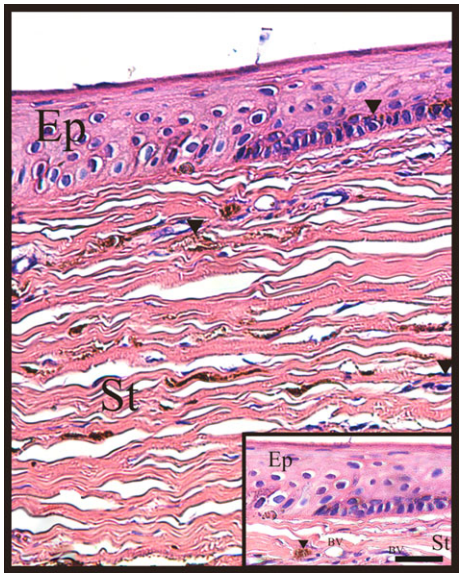

Fig. 5. Light microscopy images stained with haematoxylin–eosin: section of the peripheral cornea, with pigmented cells in basal epithelium and anterior stroma (arrowhead). Ep, epithelium; St, Stroma. Original magnification 40×. Blood vessel (BV) can be seen in the inset (Original magnification 100×, Bar 50 μm).

exhibited columnar cells with active nuclei and nucleoli surrounded by abundant cytoplasm and numerous organelles (Fig. 6b). In basal intermediate layers, the epithelial cells were round and polygonal with irregular nuclei and higher electron densities, which appeared tightly bound to each other by numerous desmosomes (Fig. 6c). Towards the surface, the intermediate cells started to elongate progressively and acquired more heterochromatin in their nuclei (Fig. 6d). In superficial layers, the flattened cells had reduced electron densities, with the nuclei exhibiting changes compatible with a disintegration process, such as membrane rupture and the chromatin being distributed irregularly (Fig. 6e). Finally, the cells in the external layer appeared to be devoid of nuclei.

Epithelial cells were anchored to the basal membrane by a continuous line of hemi-desmosomes (Fig. 7a). Below the basement membrane was a haphazardly arranged anterior stromal sheet, consistent with the Bowman's layer (Fig. 7b). The corneal stroma exhibited a characteristic orthogonal disposition of collagen (Fig. 7c) and stromal cells with cellular features of fibroblasts (Fig. 7d).

Between the stroma and the corneal endothelium, Descemet's membrane appeared as a thick acellular layer of a moderate homogeneous electron density (Fig. 7e). Finally, and lining the posterior surface of the cornea, the corneal endothelium appeared as a single layer of flat cells presenting electron-dense nuclei and cytoplasmic projections resting on the Descemet membrane (Fig. 7f).

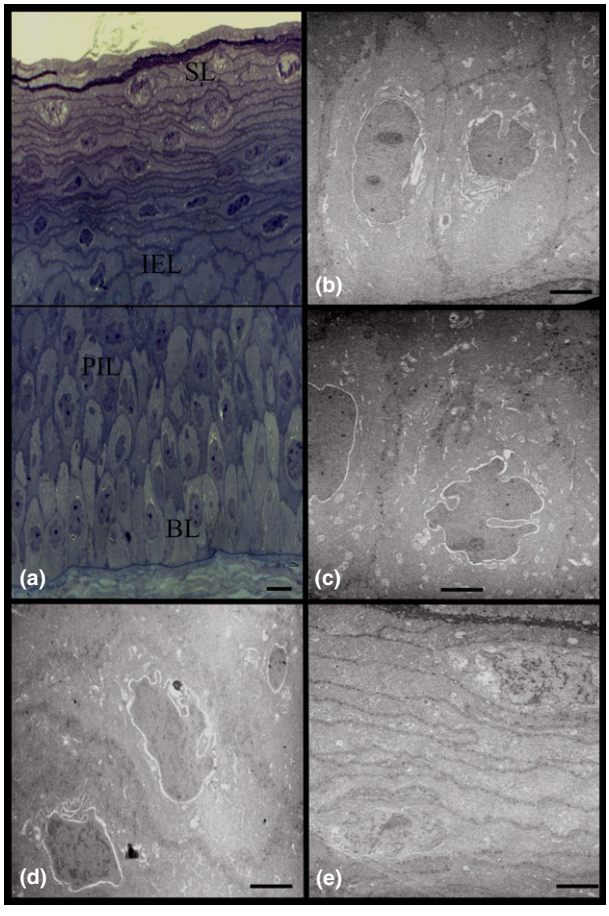

Fig. 6. Morphologic analysis of corneal epithelium. (a) semi-thin section stained with toluidine blue (a). (b–e) thin section observed by TEM. (b) columnar basal cells with low electron density; (c) polygonal intermediate with irregular nuclei and tightly bound to each other by numerous desmosomes; (d) intermediate elongated cells with more heterochromatin in their nuclei; (e) superficial cell in regression state. BL, Basal Layer; PIL, Polygonal Intermediate Layer; IEL, Intermediate Elongated Layer; Superficial Layer. Original magnifications (a): 1000×, Bars 10 μm (b–e): 3600×, Bars 200 μm.

Discussion

Slit-lamp biomicroscopy of the cornea performed before the animals were slaughtered did not disclose any corneal opacities or scars. TEM and LM studies allowed us to be able to describe and characterize some special features of the sheep corneal structures. We did not find significant differences in the thickness of the entire cornea and epithelium between young and adult animals using LM measurements. The very thick stratified epithelium, in which superficial epithelial cells showed varying degrees of cytoplasm reflectivity, indicated different metabolic conditions, a Bowman's layer that could only be observed only by TEM, a stroma, a relatively thick Descemet membrane and a single layer of endothelial cells. In Merino sheep

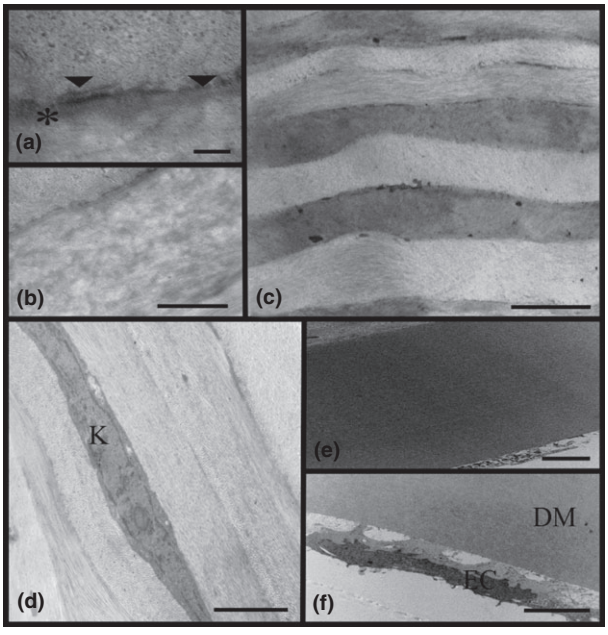

Fig. 7. Transmission electron microscopy: (a) the basal cells exhibited a continuous line of hemi-desmosomes (arrowheads) contacting with a thin and electron-dense basement membrane (*); (b) disorganized anterior stroma; (c) corneal stroma with characteristic orthogonal disposition of collagen; (d) keratocyte inter-mingled in the corneal stroma; (e) Descemet's membrane; (f) Descemet's membrane and endothelium. K, Keratocyte; DM, Descemet's Membrane; EC, Endothelial cells. Original magnifications (a): 77 500× Bars 0.2 μm, (b): 27 000× Bars 1 μm, (c–d): 4600× Bars 5 μm, (e): 3200× Bars 5 μm, (f): 4400×, Bars 5 μm.

limbus, the basal epithelial cells and keratocytes containing pigment were identified, with these results being similar to previous observations in rabbits, humans and guinea pigs, where it was assumed that the pigmentation was due to melanin granules (Lavker et al., 1991; Espana et al., 2003; Cafaro et al., 2009). The anti-oxidative activity previously reported for melanin (Prota, 1997) may serve to quench UV-induced oxidant formation in the cornea epithelium (Craitoiu et al., 2005). The absence of Bowman's layer, a less regular organization of the collagen fibrils, and the existence of blood vessels were other findings limited to the limbus area in the present study, without any superficial stromal blood vessels extending into the cornea being observed as has been previously reported in other mammal species (Dwyer et al., 1983).

Corneal confocal microscopy (CCFM) has become a useful tool during recent years for the examination of human cornea under both normal (Ruggeri and Pajaro, 2002) and pathological conditions (Jalbert et al., 2003; Tervo and Moilanen, 2003; Kobayashi et al., 2006). This technology has also been used in other studies, with data now being available on the normal corneal structures of various laboratory animals (Petroll et al., 1993; Jester et al., 2001; Grupcheva et al., 2002; Labbe et al., 2006). More recently, the morphology of living corneal layers was visualized using Heidelberg Retina Tomograph equipped with a Rostock Cornea Module for a single Pomeranian Coarsewool sheep, and other species (Reichard et al., 2010). EVCM allowed us to obtain detailed images of the central corneal layers of eyes from both young and adult Merino sheep. Unfortunately, as we only had one Heidelberg Retina Tomograph equipped with a Rostock Cornea Module for human clinical use with very limited access to animals studies, it was impossible to perform *in vivo* CCFM and to study many sheep eyes by EVCM. Despite our studies were conducted approximately 5 h post-mortem, only a few artefacts on the images were observed (increased reflectivity of the background and some alterations of the surface epithelium).

Several years ago, Muller et al. (1997) elegantly studied the post-mortem changes of human corneal nerves using LM and reported that the majority of the sub-basal nerve fibres had either degenerated or disappeared 13.5 h after death. More recently, Al-Aqaba et al. (2010) reported in an *ex vivo* CCFM human corneal nerve study that sub-basal nerve branches showed a rapid disintegration with the branching pattern significantly declining 24 h after death, whereas the stromal and limbal nerves survived during the first 5 days after death.

To our knowledge, there are no reports of corneal nerve degeneration taking place in less than 13 h post-mortem. Our images of the sub-basal nerve plexus and stromal nerve fibres were similar to the ones shown by Reichard et al. (2010) in their *in vivo* CCFM study of a Pomeranian Coarsewool sheep. In that manuscript, only the keratocyte density was reported, whereas our studies provided cellular densities of different epithelium, stroma and endothelium cells as well as that of the sub-basal nerves. In addition, our comparative study of cells and nerve density among animals of the same and dissimilar ages revealed significant differences with the density of corneal cells being significantly higher in the anterior than in the posterior epithelium and stroma. Moreover, the basal and superficial epithelial cell, stromal cell, as well as the endothelial cell densities and sub-basal nerve density, were significantly lower in adults than in young animals. The sample numbers used in our study for statistical testing were small, but higher than in Reichard et al. study, and therefore, the evidence of age-related changes should be treated with some caution. As we did not perform confocal microscopy studies of the peripheral corneal, as Patel DV and coworker did in human corneas few years ago (Patel et al., 2006), it was not possible to obtain quantitative data of the different cells in the limbus area among sheep of different ages.

Reichard et al. (2010) visualized a pronounced Bowman's layer with an approximate thickness of 10 μm, and a prominent reflective Descemet membrane partially overlapping the endothelial cells beneath, thereby making the individual cells almost indistinguishable. In contrast, we observed Descemet's membrane to be a dark transition zone between the posterior stroma and the endothelial cells, with Merino sheep endothelium being seen as a regular polygonal monolayer of cells which could be accurately counted. The reflective stellate-shaped keratocytes in sheep were similar in shape but smaller than those found previously in rat and mice corneas (Labbe et al., 2006). Summing-up, this is the first report of a detailed ultrastructural description of corneas from young and adult healthy female Merino sheep. Qualitative as well as quantitative data of the different components of the cornea are provided using corneal confocal microscopy, transmission electron microscopy and conventional histology. This increased knowledge about normal sheep cornea will permit a better understanding and interpretation of pathological changes occurring in sheep.

Acknowledgements and Funding

None of the authors has any financial or personal relationships that could inappropriately influence or bias the content of the study. This work was supported by the following Argentinean grants: CONICET PIP: 112-200801-01455, and SECYT UNC.

References

Al-Aqaba, M. A., T. Alomar, A. Miri, U. Fares, A. M. Otriand, and H. S. Dua, 2010: Ex vivo confocal microscopy of human corneal nerves. Br. J. Ophthalmol. **94**, 1251–1257.

Cafaro, T. A., S. G. Ortiz, C. Maldonado, F. A. Esposito, J. O. Croxatto, A. Berra, O. L. Ale, J. I. Torrealday, E. A. Urrets-Zavalía, J. A. Urrets-Zavalía, and H. M Serra, 2009: The cornea of Guinea pig: structural and functional studies. Vet. Ophthalmol. **12**, 234–241.

Cardellino, R. C., 1989: Sheep Breeding Programmes in Uruguay. Braz. J. Genet. **12** (3 Suppl), 95–106.

Craitoiu, T., C. Mocanu, D. Barascuand, and O. Cristian, 2005: [Histological particularities of sclerocorneal limbus–implications in ocular pathology]. Oftalmologia **49**, 86–92.

Dwyer, R. S., S. Darougarand, and M. A. Monnickendam, 1983: Unusual features in the conjunctiva and cornea of the normal guinea-pig: clinical and histological studies. Br. J. Ophthalmol. **67**, 737–741.

Espana, E. M., A. C. Romano, T. Kawakita, P. M. Di, R. Smiddyand, and S. C. Tseng, 2003: Novel enzymatic isolation of an entire viable human limbal epithelial sheet. Invest. Ophthalmol. Vis. Sci. **44**, 4275–4281.

Galan, A., E. M. Martin-Suarezand, and J. M. Molleda, 2006: Ophthalmoscopic characteristics in sheep and goats: comparative study. J. Vet. Med. A Physiol. Pathol. Clin. Med. **53**, 205–208.

Grupcheva, C. N., W. T. Laux Fenton, C. R. Greenand, and C. N. McGhee, 2002: In vivo and ex vivo in situ confocal analysis of a rat model demonstrating transient 'epithelialization of the endothelium'. Clin. Experiment. Ophthalmol. **30**, 191–195.

Guyomard, J. L., S. G. Rosolen, M. Paques, M. N. Delyfer, M. Simonutti, Y. Tessier, J. A. Sahel, J. F. Legargasson, and S. Picaud, 2008: A low-cost and simple imaging technique of the anterior and posterior segments: eye fundus, ciliary bodies, iridocorneal angle. Invest. Ophthalmol. Vis. Sci. **49**, 5168–5174.

Jalbert, I., F. Stapleton, E. Papas, D. F. Sweeney, and M. Coroneo, 2003: In vivo confocal microscopy of the human cornea. Br. J. Ophthalmol. **87**, 225–236.

Jester, J. V., L. Y. Ghee, J. Li, S. Chakravarti, J. Paul, W. M. Petroll, and H. Dwight Cavanagh, 2001: Measurement of corneal sublayer thickness and transparency in transgenic mice with altered corneal clarity using in vivo confocal microscopy. Vision. Res. **41**, 1283–1290.

Kobayashi, A., H. Yokogawa, and K. Sugiyama, 2006: In vivo laser confocal microscopy of Bowman's layer of the cornea. Ophthalmology **113**, 2203–2208.

Labbe, A., H. Liang, C. Martin, F. Brignole-Baudouin, J. M. Warnet, and C. Baudouin, 2006: Comparative anatomy of laboratory animal corneas with a new-generation high-resolution in vivo confocal microscope. Curr. Eye Res. **31**, 501–509.

Lavker, R. M., G. Dong, S. Z. Cheng, K. Kudoh, G. Cotsarelis, and T. T. Sun, 1991: Relative proliferative rates of limbal and corneal epithelia. Implications of corneal epithelial migration, circadian rhythm, and suprabasally located DNA-synthesizing keratinocytes. Invest. Ophthalmol. Vis. Sci. **32**, 1864–1875.

Muller, L. J., G. F. Vrensen, L. Pels, B. N. Cardozo, and B. Willekens, 1997: Architecture of human corneal nerves. Invest. Ophthalmol. Vis. Sci. **38**, 985–994.

Patel, D. V., T. Sherwin, and C. N. McGhee, 2006: Laser scanning in vivo confocal microscopy of the normal human corneoscleral limbus. Invest. Ophthalmol. Vis. Sci. **47**, 2823–2827.

Patel, D. V., J. Y. Ku, R. Johnson, and C. N. McGhee, 2009: Laser scanning in vivo confocal microscopy and quantitative aesthesiometry reveal decreased corneal innervation and sensation in keratoconus. Eye (Lond). **23**, 586–592.

Petroll, W. M., H. D. Cavanagh, and J. V. Jester, 1993: Three-dimensional imaging of corneal cells using in vivo confocal microscopy. J. Microsc. **170**, 213–219.

Prince, J. H., C. D. Diesem, I. Eglitis, and G. Ruskell, 1960: The Sheep. In: Anatomy and Histology of the Eye and Orbit in Domestic Animals. (University of Michigan eds). Illinois: Charles C Thomas, pp. 182–206.

Prota, G., 1997: Pigment cell research: what directions? Pigment Cell Res. **10**, 5–11.

Reichard, M., M. Hovakimyan, A. Wree, A. Meyer-Lindenberg, I. Nolte, C. Junghans, R. Guthoff, and O. Stachs, 2010: Comparative in vivo confocal microscopical study of the cornea anatomy of different laboratory animals. Curr. Eye Res. **35**, 1072–1080.

Ruggeri, A., and S. Pajaro, 2002: Automatic recognition of cell layers in corneal confocal microscopy images. Comput. Methods Programs Biomed. **68**, 25–35.

Scott, J. E., and T. R. Bosworth, 1990: A comparative biochemical and ultrastructural study of proteoglycan-collagen interactions in corneal stroma. Functional and metabolic implications. Biochem. J. **270**, 491–497.

Tervo, T., and J. Moilanen, 2003: In vivo confocal microscopy for evaluation of wound healing following corneal refractive surgery. Prog. Retin. Eye Res. **22**, 339–358.